Peer-reviewed version available at *Coatings* **2018**, *8*, 129; doi:10.3390/coatings8040129

Investigation of Element Effect on High Temperature Oxidation of HVOF NiCoCrAlX Coatings

Pimin Zhang[1*], Ru Lin Peng[1], Xin-Hai Li[2], Sten Johansson[1]

1 Department of Management and Engineering, Linköping University, 581 83, Linköping, Sweden

2 Siemens Industrial Turbomachinery AB, SE-61283 Finspång, Sweden

*Corresponding author: pimin.zhang@liu.se

Abstract:

MCrAlX (M: Ni or Co or both, X: minor elements) coatings have been widely used to protect hot components in gas turbines against oxidation and hot corrosion at high temperatures. Understanding the influence of the X-elements on oxidation behaviour is important in the design of durable MCrAlX coatings. In this study, NiCoCrAlX coatings doped with Y+Ru and Ce, respectively, were deposited on Inconel-792 substrate by HVOF. The samples were subjected to isothermal oxidation test in laboratory air at 9000, 1000, 1100 ºC and cyclic oxidation test between 100 ºC and 1100 ºC with 1 hour dwell time at 1100 ºC. It was observed that the coating with Ce shows a much higher oxidation rate than the coating with Y+Ru under both isothermal and cyclic oxidation tests. Besides, β-depletion due to interdiffusion between coating and substrate was significantly lower with Ru addition. Simulations results using both a moving phase boundary model and an established oxidation-diffusion model show that Ru stabilize β grains which reduces β-depletion of coating due to substrate interdiffusion. This paper presents a comprehensive study of the influence of Ce and Ru on oxidation behaviour including investigation of the microstructure evolution influenced by oxidation time at coating surface and coating-substrate interface combining experiment and simulation results.

Keywords: MCrAlX coatings; Ruthenium; Cerium; Oxidation; Simulation.

1. Introduction

MCrAlX coatings (M for Ni and/or Co, X for minor elements) are widely used to protect the superalloys against high-temperature oxidation and hot corrosion in gas turbine engines. The protection offered by MCrAlX coatings against high-temperature oxidation relies on the performance of a thermally grown oxide (TGO) scale formed at the coating-

gas interface [1,2]. A continuous and dense α-Al_2O_3 of hexagonal close-packed structure is desired for its resistance against diffusion of oxygen ions as well as high thermal and chemical stabilities [1]. The growth of alumina scale at the coating surface and substrate interdiffusion depletes Al-rich β phase in MCrAlX coatings, which serves as Al reservoir during oxidation. By modifying these two processes, β phase depletion rate can be reduced, therefore improved coating oxidation performance can be achieved by doping elements, such as Y [3,4], Hf [5,6], Ta[7], Re[8] and so on.

Comparing with isothermal oxidation, cyclic oxidation induces thermal stress on TGO, resulted in TGO spallation [9]. The addition of varies reactive elements (Y, Hf, Ce) to alloys and coatings can remarkably improve spallation resistance in cyclic oxidation by anchor effect. Among all reactive elements, Cerium (Ce) effect in improving oxidation performance has drawn attentions in recent years. It was reported that the adherence of the oxide film formed on Ni-20Cr alloys was improved by small additions of Ce and Si by the formation of root shape protrusions which inhibits the crack propagation at TGO and increases the spallation resistance [10,11]. On the other hand, substrate interdiffusion between coating and substrate also depletes β phase, which is greatly dependent on coating composition, substrate composition, and oxidation temperature [12–14]. The reduction of inwards diffusion of Al from coating to substrate may significantly extend the life of MCrAlX coatings. It is reported that by deposition a Ru layer between coating and substrate effectively slowed down the inward diffusion of Al by the formation of a (Ru,Ni)Al layer as diffusion barrier [15]. Besides, the addition of Ru in Ni-base superalloys is also beneficial since it decreases the precipitation and growth rate of topologically close-packed (TCP) phases, which prevents the degradation of mechanical properties [16].

The overall oxidation resistance is closely related to the coating composition and a large number of publications have been dedicated to studying the effect of minor addition of alloying elements [14,7,17,8,18,19]. However, no effort has been made to compare the capabilities of improving cyclic oxidation resistance between Ce and other reactive elements (REs) like Y; and the effect of Ru doping in MCrAlX coating on substrate interdiffusion has rarely been discussed. The current work covers two parts: 1) a

Peer-reviewed version available at Coatings 2018, 8, 129; doi:10.3390/coatings8040129

comparative research is carried out on high velocity oxygen fuel (HVOF) sprayed coatings at isothermal oxidation and cyclic oxidation tests to study Ce effect on cyclic oxidation resistance; 2) Ru effect on stability of β phase and Al interdiffusion is studied using both short-range and long-range model to simulate the phase evolution and interdiffusion in coating-superalloy systems [19–21]. This paper aims at increasing understanding the effects of Ru and Ce on the behaviour of MCrAlX coatings during high temperatures oxidation.

2. Materials and experiment

In the present study, two NiCoCrAlX powders were tailor-made by Beijing General Research Institute of Mining with the size range: -37 μm for C1 and -53+30 μm for C2. NiCoCrAlX coatings were deposited on Inconel 792 substrate (composition by wt. %: 12.5 Cr, 9 Co, 4.2 W, 4.2 Ta, 4 Ti, 3.4 Al, 1.9 Mo 0.08 C, 0.03 Zr+B, balanced by Ni), using the JP5000 HVOF spray system. The NiCoCrAlX coating thickness were measured around 200 μm with the coating roughness in the range between 6 and 6.5 μm. Prior to coating deposition, the substrate surfaces were grit blasted. After the deposition, specimens were subjected to a heat treatment, including solution annealing at 1120 °C for 2 hours in vacuum, followed by aging treatment at 845 °C for 24 hours in air and air cooling to room temperature. Such a heat treatment, which is intended for strengthening the IN-792 substrate [22], also increases the bond strength between the coating and substrate [23]. The chemical composition of the heat-treated MCrAlX coatings was measured on the average of 20*25 μm cross-section area by the combination of energy dispersive spectroscope (EDS) and wavelength dispersive spectroscope (WDS), as listed in Table 1.

Long-time isothermal oxidation tests on the coated specimens at 900 and 1000 °C were performed to simulate the oxidation behaviour which is close to service temperature of MCrAlX coating in gas turbine component; cyclic oxidation tests were conducted in laboratory air to compare with isothermal oxidation tests at 1100 °C to study coating cyclic oxidation resistance, see Table 2 for details. One cycle of the cyclic oxidation consisted of heating at 1100 °C for 1 hour and forced-air cooling to 100 °C in 10 min. After oxidation, oxidized samples were mounted in epoxy and polished. The surface and the cross-sections

of the specimens were examined using a Hitachi SU70 FEG scanning electron microscope (SEM) for microstructure observation and chemical composition measurement. To better describe the microstructure development, the coating are separated into several zones, including: outer-β-phase depletion zone (OBDZ), β-phase left zone (BLZ), inner-β-phase depletion zone (IBDZ), as illustrated in Fig. 1. The evolution of different areas according to Fig. 1 were quantified by image analysis software.

3. Simulation

To have a better understanding of the mechanism behind the effect of Ru on Al diffusion behaviour, the experiment work was supplemented with computational simulation, using Thermo-Calc software package with the advanced Ni-base thermodynamic database TCNI8 [24] and corresponding mobility database MONI4 [25]. Firstly, to investigate the influence of Ru addition in MCrAlX coatings, Ru and Al solubility in the constituent β and γ phases and the corresponding phase equilibrium were calculated using Thermo-Calc. Secondly, Ru effect on Al diffusion between localized β and γ grains were investigated by a short-range diffusion calculation using the moving phase boundary model in DICTRA [26]. Finally, a long-range interdiffusion simulation between coating and substrate using an established model [13,19,20] based on DICTRA was performed to demonstrate the aforementioned Ru effect on Al diffusion. The models are introduced below in 3.1 and 3.2, respectively.

3.1 Short-range diffusion

To study the Ru effect on Al diffusion between β and γ phase, a 1-D moving phase boundary model which has been incorporated in DICTRA software [26] was adapted to simulate the short range diffusion behaviour. The model is based on the diffusion controlled growth under local equilibrium conditions as suggested by Larsson and Reed [27]. A more intimate and comprehensive description can be found in Ref [28]. The assumption for this model includes: 1) planar geometry corresponding to an infinitely wide plate of a certain thickness, 2) sharp interface with local equilibrium, 3) diffusion controls the movement of the phase boundary, 4) zero-flux at the boundary. The utilization of such a model to simulate diffusion in MCrAlX coating can be useful to investigate: 1) the

Peer-reviewed version available at Coatings 2018, 8, 129; doi:10.3390/coatings8040129

movement of interfacial β/γ phase boundary and 2) the local diffusion behaviour of Al between β and γ phase at short time since no flux is introduced into the system. The model includes the diffusion process through the interface between two regions (the γ phase region on the left side and the β phase region on the right side) and phase equilibrium calculation for each region. The region length, 5.5 for γ and 4.5 μm for β, were measured from the average grain size on the heat-treated samples. A double grit structure was set with a set of non-linear nodes for each region with a geometry factor of 0.9 (linear grid when geometry factor is 1), which gives a distribution of nodes: denser close to the interface and thinner near the outer region boundaries. The composition of the phases was stored in each node. The composition profile in the γ and β regions was linear, which was taken either from EDS measurement of as-received samples or from equilibrium calculation of corresponding coating composition by Thermo-Calc.

3.2 Long-range diffusion

A brief description of the oxidation-diffusion model for the simulation of long range diffusion is given here, while a more detailed description can be found in Refs [11,15,19]. The substrate and coating compositions were represented in 1D by a set of non-linearly distributed nodes (dense near the interface, coarse in the substrate), in which the local composition is stored. In this paper, the nominal compositions in Table 1 were used as input data. The simulation of oxidation and diffusion followed an iterative process where each iteration included: step 1 - Al removal from the coating surface to simulate Al depletion at coating surface due to the formation of alumina using a MATLAB script, and step 2 – phase equilibrium calculation and substrate interdiffusion simulation using DICTRA software. The obtained compositions were then used as input data for the next loop.

4 Results and Discussion

4.1 Experimental results analysis

4.1.1 Heat-treated coating

Peer-reviewed version available at Coatings 2018, 8, 129; doi:10.3390/coatings8040129

The cross section of heat treated coatings and EDS mapping results are shown in Fig. 2 and Fig. 3 for C1 and C2 coating, respectively. A characteristic splat-on-splat structure can be seen with pores and cracks marking the splat's boundaries. After the solution and aging heat treatment, a typical β+γ microstructure formed in coatings (β phase in grey). The EDS mapping results are shown in Fig. 2b, Ru has a similar pattern as Al indicating Ru has a higher solubility in β phase than in γ phase, which is also confirmed by EDS point analysis showing that 4.8 wt% Ru in β phase, compared with 1.1 wt% Ru in γ phase. Y and Ce were mainly segregated to the splat's boundary according to EDS mapping (Fig. 2b and Fig. 3b) due to their affinity for oxygen.

4.1.2 Thermally grown oxide microstructure

The formation and growth of TGO play an important role in its subsequent thickening [29], therefore the oxidation behaviour of coatings can be evaluated by studying the TGO growth behaviour. Figs. 4-7 show the cross-sectional microstructure of alumina scale formed on coating surface at different oxidation temperature. In general, a two-layer structure of alumina scale was observed: outer porous layer and inner dense layer. Besides, spinel could also be found covering alumina scale, as shown in Figs. 5-7. However, the microstructure of alumina scale is greatly dependent on the oxidation temperature. In Figs 4a and 4c for 900 °C oxidation, a thick blade-like outer alumina layer and a thin dense inner alumina layer was observed with their boundaries marked in dash line. The formation of blade-like Al_2O_3 resulted from the fast outward growth of θ-Al_2O_3 for short exposure time at relatively low temperature (900 °C), which later transformed into α-Al_2O_3, as suggested by Liu et al. [30]. Since the growth rate of θ-Al_2O_3 is 10 times faster than α-Al_2O_3 [31,32], the inner alumina layer grows inward much slower than the outward growth of θ-Al_2O_3. Eventually, a two layer structure of alumina scale consisted of a thick porous outer layer transformed from fast grown θ-Al_2O_3 and an inner slow grown α-Al_2O_3 was observed. The formation of pores in outer alumina layer gives evidence for the θ-to-α Al_2O_3 transformation due to the volume reduction, which then incorporated in outer layer upon further alumina scale development [33,34]. With the increasing oxidation time to 5000 h, the main alumina growth mechanism shifted from outward grown outer layer to inward growth of inner alumina layer, as indicated by the similar outer layer thickness and the obvious thickening

Peer-reviewed version available at Coatings 2018, 8, 129; doi:10.3390/coatings8040129

of inner layer after 5000 h oxidation. The outer layer of two coatings show similar morphology and thickness, indicating a similar outward growth behavior of outer layer of two coatings. Y-rich oxides incorporated inner layer of Y-rich C1 coating in Fig. 4b is thicker than that of C2 for 5000 h oxidation, resulted from the formation of Y-rich oxide in alumina provide fast diffusion path for Al [18,29,35–37]. However, no such effect could be observed on Ce-doped C2 coating, indicating the addition of Ce in MCrAlX coating doesn't modify the Al diffusion in alumina scale.

Fig. 5 shows the cross section of TGO formed on C1 and C2 coatings after isothermal oxidation at 1000 ºC for different oxidation time, showing the TGO consisted of spinel, outer alumina layer and inner alumina layer. A thin outer layer and a columnar inner layer alumina scale could be observed on C1 coating. However, alumina scale formed on C2 coating consisted of a thick porous outer layer and an equaxial inner layer. Upon further oxidation to 5000 h, the thickening of inner layer in C1 dominates the overall growth of alumina scale after 50 h oxidation, indicated by the relatively similar outer layer thickness. Fig. 6 shows EDS mapping of alumina scale formed on C1 coating after 5000 h oxidation at 1000 ºC, Y-rich oxides incorporated in alumina scale can be readily observed, no Ru or Ce could be identified in TGO by EDS. The formation of columnar structure of inner alumina layer in C1 resulted from the segregation of Y-rich oxide at alumina grain boundaries accelerates the Al grain boundary diffusion, which aids the formation of columnar structure [38]. No such influence from Ce addition in C2 can be observed. Besides, the much thicker porous outer layer in C2 coating compared to C1 indicates that the addition of Y in MCrAlX coatings suppresses the growth of θ-Al_2O_3 and enhances the fast development of dense α-Al_2O_3 layer. However, the addition of Ce in MCrAlX coatings shows no positive effects as that of Y. Similar TGO microstructure can be observed on C1 and C2 coatings after isothermal oxidation at 1100 ºC for different oxidation time, as illustrated in Fig. 7. It's worthy to mention that the outer alumina layer thickness of C2 reached half of the overall alumina scale thickness at 800 h oxidation, indicating not only the inward growth of inner alumina layer but also the growth of outer layer contribute to the overall alumina scale growth in C2 coating, on the contrary, the influence of outer

alumina layer growth on the overall alumina growth is trivial in C1 considering the relatively thin out layer thickness of C1 without much thickening after 800 h oxidation.

4.1.3 Oxidation kinetics

The development of the outer beta phase depletion zone (OBDZ), which appeared in the coatings below the coating-oxide interface (Fig. 1), is directly connected to the loss of Al due to surface oxidation. The OBDZ growth rate was used to represent oxidation resistance of coatings instead of TGO growth rate. As is recognized, the growth of OBDZ thickness, which represents the growth of alumina scale, is assumed to be diffusion-controlled following a parabolic oxidation law:

$$h = (kt)^{1/2}, \quad (1)$$

with k following the Arrhenius relationship:

$$k = k_0 e^{-\frac{Q}{RT}}, \quad (2)$$

where h represents OBDZ thickness, k is the growth rate constant, t denotes oxidation time, Q is the activation energy, T is temperature and R is gas constant 8.314 $Jmol^{-1}K^{-1}$.

Fig. 8 shows the evolution of OBDZ thickness during oxidation against square root of oxidation time at different temperature. As can be seen, the fitting of regression models shows good correspondence with the experimental data, with coefficients of determination (R^2) higher than 0.95. At 900 °C, the OBDZ thickness is quite large at 500 h for C2 coating, which developed slower compared with that of C1. It corresponds to the microstructural observation in Fig. 4 that the outward growth of transient alumina on C2 coating reached a certain thickness at short time, resulted in a fast Al depletion (thick OBDZ) at 500 h. Once the transient alumina fully transformed into α-Al_2O_3, the overall growth of alumina scale shifted to inward growth of inner alumina layer. Due to the aforementioned Y effect, the inner layer of C1 coating grew faster than that of C2 coating, where Ce shows no such effect, leading to a faster overall alumina scale growth rate of C1 coating. In the case of 1000 °C oxidation (Fig. 5), the growth of inner layer dominates the overall growth of alumina scale in C1. However, the growth of outer porous layer of C2 also contributes to

the overall growth of alumina scale, giving a similar OBDZ growth rate. At 1100 °C, the larger OBDZ thickness growth rate of C2 coating indicates that both inner and outer alumina layer contribute to the overall growth rate of alumina scale, leading to a larger growth rate of C2 than that of C1.

The temperature dependence of OBDZ thickness growth rate constants were obtained from the slope of straight lines by fitting Eq. (1) to the experimentally determined OBDZ thickness growth data in Fig. 8a, b and c. It is apparent that the Arrhenius type (see Eq. (2)) temperature dependence applies in the evolution of OBDZ thickness in both C1 and C2 coatings. In Fig. 8d the logarithm of the OBDZ rate constants k of the C1 and C2 coatings were plotted against the inverse of temperature $10^4/T$. Both rate constants are in good agreement within this experiment range. It reflects the growth of Al_2O_3 scale, since the Al in OBDZ is mostly consumed by the formation of alumina scale. From the slope in Fig. 8d, the activation energy of OBDZ growth were found to be approximately 311 kJ/mol for C1 coating. It is noted that the activation energy of C1 is comparable with activation energy of α-Al_2O_3 growth of sputtered NiCrAlY (390 kJ/mol) [39] and that of NiAl (382 kJ/mol) [31], however considerably less than that of Al lattice diffusion in Al_2O_3 (~500 kJ/mol) [40]. Most evidence indicates that the growth of Al_2O_3 scale of C1 coating is dominated by grain-boundary diffusion of oxygen [39]. Also, the presence of Y may reduce the kinetics of Al lattice diffusion, which has been reported in [41]. However, the activation energy of C2 coating is 619 kJ/mol, which is even larger than the activation energy of Al lattice diffusion in Al_2O_3. It can be explained that the growth of outer transient alumina layer has a great impact on the overall growth of alumina scale in C2 coating, indicated by the relatively thick outer alumina layer of C2 at different oxidation temperature. The shifting of dominant growth mechanisms from outward growth outer layer to inward growth of inner layer in C2 coating alter the growth rate of C2 coating especially at 900 °C, which cause a deep slop in Fig. 8 giving a much higher activation energy of C2 coating. Thus, the addition of Y suppress the growth of outer layer and modify the overall alumina growth mechanism, on the contrary, the addition of Ce doesn't modify the alumina scale growth, leading to a mutual growth of both outer and inner alumina layers, therefore a much higher oxidation activation energy.

4.1.4 Comparison of oxide scale adhesion

The spallation of oxide scale will accelerate the consumption of Al, which leads to fast depletion of β-phase in the coating, and thus a comparison of the OBDZ growth rate between isothermal and cyclic oxidation tests can be used to evaluate the spallation resistance of the oxide scale. Figs. 9a and 9b show the OBDZ thickness changes of the Y+Ru-doped C1 coating and Ce-doped C2 coating during cyclic oxidation testing at 1100 °C, and isothermal oxidation testing at 1100 °C, respectively. The results were obtained by measuring the thickness evolution of OBDZ with oxidation time.

From Fig. 9, it can be seen that for the C2 coating the OBDZ thickness after 800 cycles in cyclic oxidation test (85.1±5.9 μm) was 3.6 folder of that after 800 h isothermal oxidation test (23.6±1.5 μm). For the C1 coating, the OBDZ thickness difference between isothermal oxidation (17.2±3.0 μm) and cyclic oxidation (44.7±3.3 μm) was much smaller. As no obvious TGO spallation was observed under isothermal oxidation test, the accelerated OBDZ growth rate observed in the cyclic oxidation test for both coatings was mainly related to TGO spallation due to thermal stresses induced by the temperature changes. The much larger OBDZ thickness of the C2 coating, twice of that of the C1 coating, after 800 cycles indicated a poorer spallation resistance of the former. There is no doubt that a significant difference exists between Y+Ru and Ce dopants in improving the scale adhesion. Ogawa et al. [42] observed root-like oxide precipitates in the TGO in coatings containing Ce, which improved the TGO adhesion due to an anchor effect, and the influence was found to become more pronounced when the amount of Ce increased. However, no such root-like oxide precipitates were found in the TGO in the Ce-doped C2 coating. This could be due to a too small amount of Ce addition (0.2 wt. %) compared with Ogawa's work (0.5, 1, 1.5 wt. %). Therefore, considering its poor isothermal oxidation and cyclic oxidation resistance, C2 coating with 0.2 wt. % Ce doping could not provide as good oxidation resistance as 0.3 wt. % Y-doped C1 coating.

4.2 Simulation results

Based on EDS analysis that no Ru in the TGO layer, and the low activation Ru-oxide formation energy 94.25 kJ/mol compared to 847.25 kJ/mol that of Al_2O_3 at 1000 °C, it is reasonable to assume that Ru has no direct influence on the surface oxidation of the coatings. The beneficial effect of Ru on prolonging the coating lifetime derives from its effect on reducing the loss of Al to the substrate through interdiffusion, which was observed in C1. As Fig. 1 shows the inner beta phase depletion zone in C1 is much smaller than that in C2. Results from the different simulations to explore the mechanisms behind the Ru effect are presented below.

4.2.1 Phase equilibrium calculation

Since the simulation is based on the combination of diffusion and phase equilibrium calculation, the effect of Ru on the interdiffusion was further investigated by phase equilibrium calculation using Thermo-Calc, see Fig. 10. Several different alloy systems with similar compositions to the C1 coating were chosen: staring with Ni27Co15Cr12.5Al+1Ru (in wt%) and then increasing Ru to 3.5Ru with step size of 1 wt% of Ru at the expense of Ni. It's clear that the β-phase fraction decreased with the decreasing Ru concentration in the alloy, from 74 % to 71.5 % at 1100 °C, indicating that Ru stabilizes the β-phase in the alloy systems. This result is consistent with [19], which claimed that Ru greatly stabilizes β-phase by largely extending the β-phase field in the phase diagram.

4.2.2 Short range diffusion

The moving phase boundary model was applied to simulate short-range diffusion through the γ/β phase boundary in the coating for two coating systems, named S1 and S2 under high temperature exposure. The chemical composition of the γ and β phases in S1 and S2, given in Table 3, were based on EDS measurements of the heat treated coating C1 and C2, respectively. The chemical gradient of other minor elements, such as Si, Mo and Ta was neglected in order to highlight the influence of Ru on the short-range diffusion between the γ and β phases and to accelerate the simulation speed as well.

Fig. 11.shows the interfacial position (phase boundary) movement of the S1 and S2 systems with time for up to 10^7 s at 1100 °C (Note that the original phase boundary for both S1 and

S2 were at 5.5 μm, and 800 hr is $2.88*10^6$ s). It can be seen that the interfacial position of both S1 and S2 changed with time and reached a new equilibrium state after 10^5 s due to no interference from outside the system. Comparing between S1 and S2, the interfacial position moved by 0.4 μm towards the γ phase region for S1 but 0.8 μm towards the β phase region for S2. This means that the β phase region had the tendency to grow in S1 but to shrink in S2.

Fig. 12 shows the calculated Al concentration profiles of the S1 and S2 systems at 0 s and 10^5 s, Al concentration profiles at other time were not included as they were close to the data at 10^5 s. The γ phase region and β phase region were arranged from left to right in the moving phase boundary model, and the interface was set at a distance=5.5 μm. The concentration of Al in β decreased with increasing time in both systems. For the S1 (Fig. 12a), the Al concentration in γ increased only by 0.6 wt. % which, along with the decrease of Al in β and the expanding of the β phase region, indicates only a small amount of Al diffused from β into γ. For the S2 (Fig. 12b), however, the diffusion of Al from β into γ led to an increase of Al by 1.8 wt. % in the γ phase. According to the Thermo-Calc calculation, the diffusivity of Al in γ and β phase for the S1 and S2 are $4.9*10^{-13}$ and $9.7*10^{-14}$ m^2/s, respectively. Hence, from the analysis above, Al in the S2 system diffused from β into γ rapidly, which means the inward diffusion of Al from coating to substrate is faster in S2 as Al diffusivity in the γ phase is higher than in the β phase. Thus, the addition of Ru in the C1 coating stabilizes β and slows down β phase depletion.

The difference of Al solubility in β phase of C1 and C2 coating can explained by the Ru effect. The Al and Ru concentrations in the γ and β phases from EDS measurements on C1 and C2 coatings after heat treatment are listed in Table 4. A slightly higher Al concentration was shown for the C2 coating containing Ce. The influence of Ru on the Al solubility in the β phase at various temperatures was also calculated using Thermo-Calc and the initial composition of C1 coating as input. The results shown in Fig. 13 are the projection of three-dimensional diagram with weight percent of Al and Ru, namely the solubility of Al and Ru, in the β phase as x and y-axis and temperature as z-axis. The temperature was marked selectively in the diagram. The solubility of Al increased with increasing Ru solubility,

from 17.5 wt. % at 1200 °C to 18.1 wt. % at 1080 °C, and it reached 17.9 wt.% at the maximum solubility of Ru, 6.56 wt. % in β. According to the equilibrium calculation, the increasing enrichment of Ru in β phase will enlarge the solubility range of Al in the β phase. Thus, the increasing amount of Ru in β phase would aid the partition of Al in β phase.

4.2.3 Long range diffusion

Interdiffusion between the coating and substrate can result in β-depletion near the coating-substrate interface in the coating side (Fig. 3) as aluminium moves from the coating to the substrate. The β-phase depletion rate, controlled by diffusion, is expected to follow Eq. (1). To demonstrate Ru effect on the phase equilibrium and diffusion which has been mentioned in previous sections, the long-range diffusion between coating and substrate were simulated using the oxidation-diffusion model by studying the β-phase depletion rate.

Fig. 14a shows the simulation results of β phase depletion for the Y+Ru-doped C1 coating at 1100 °C. Simulation was also performed for the C2 coating but the results are not presented here. Fig. 14b plots both the isothermal 1100 °C oxidation test data and simulation data of IBDZ (inner β-depletion zone, 14a) thickness against square root of time. The IBDZ growth rates of C1 and C2 coatings were 1.44 and 2.17 μm/$h^{0.5}$, respectively, which were consistent with the simulation results (1.52 μm/ $h^{0.5}$ for C1 and 2.05 μm/ $h^{0.5}$ for C2). Thus, both simulation and experimental analyses showed that the addition of Ru in C1 coating decreased interdiffusion induced β-phase depletion. DICTRA simulation is based on the coupling of phase equilibrium calculation and the solving of Fick's law on each small time steps and nodes. And the element diffusivity data in oxidation-diffusion model is essential to solve the Fick's law, which derived from the calculation of effective diffusivity of each element according to homogenization model 5 in DICTRA. Thus, the long-range diffusion simulation is actually the comprehensive coupling of element effect on both phase equilibrium and diffusion behaviour. Since the simulation results agreed well with experimental results and the IBDZ growth rate of C1 is lower than C2, the profound effect of Ru on stabilizing β phase and its effect on decreasing short range diffusion can be

proved by the long-range diffusion simulation. Therefore, Ru effect on retarding the long range diffusion of Al between coating and substrate can be inferred.

In summary, the simulations on both short range and long range diffusion demonstrated that Ru addition in the NiCoCrAlX coating increased Al solubility in the β phase as well as the β phase fraction. Due to a higher diffusivity of Al in γ phase than β phase, these two effects both contributed to stabilize the β phase and slow down the inward diffusion of Al from coating to substrate.

5. Conclusion

Oxidation behaviour of NiCoCrAlX coatings with Ce and Y+Ru additions was compared at different test conditions. Conclusions can be drawn as follows:

1. A two layer structure alumina scale developed in the TGO of both Y+Ru doped coating and Ce-doped coating: an outer porous outward grown layer, and an inner oinward grown layer. The continued growth of the outer and inner of Al_2O_3 layer depleted Al from the coatings, and the growth behaviour of the two layer differed at different temperature, which is also dependent on coating composition.
2. Comparison of the activation energy for OBDZ growth with that for Al lattice diffusion in Al_2O_3 indicates that the growth of alumina scale in Y+Ru-doped coating is dominated by grain boundary diffusion of oxygen with the positive effect of Y to increase the growth kinetics of alumina scale. However, Ce-doped coating shows a different alumina scale growth kinetics.
3. In comparison with the Ce-doped coating, the Y+Ru-doped coating showed a lower growth rate of the outer β-depletion zone (below the protective scale) in both isothermal 1100 ^{0}C and cyclic oxidation tests, indicating a better resistance to oxide growth and a stronger adhesion of TGO. And the spallation of alumina scale in Ce-doped coating at 1100 ^{0}C accelerated the consumption of Al in coating.
4. The addition of Y in MCrAlX coatings plays an important role during coating oxidation, including modifying alumina growth mechanisms, aiding the columnar alumina microstructure formation, increasing alumina scale adhesion against spallation. However, none of such positive effects can be observed by the addition of

Ce in MCrAlX coating. Therefore, it is reasonable to assume that the addition of Ce can't replace the important role of Y in MCrAlX coatings.

5. The Y+Ru-doped coating exhibited a lower growth rate of inner β-depletion zone (near the coating-substrate interface) induced by interdiffusion. The simulation results show that the addition of Ru increases the solubility of Al in the β phase and the β phase fraction, which reduce the loss of Al due to interdiffusion and stabilize the β phase.
6. While the addition of about 3.3 wt. % Ru seems to significantly increase resistance against interdiffusion, the substitution of Y (0.3 wt. %) by a similar amount of Ce (0.2 wt. %) decreases greatly the oxidation resistance at the coating surface.

Acknowledgment

The author would like to greatly acknowledge Siemens Industrial Turbomachinery AB (Finspång, Sweden) for all contributions to this project, and Swedish Energy Agency through KME consortium - ELFORSK for their financial support. The project teams at Linköping University are also acknowledged for their support on this research.

Reference

[1] W. Brandl, D. Toma, J. Krüger, H.J. Grabke, G. Matthäus, The oxidation behaviour of HVOF thermal-sprayed MCrAlY coatings, Surf. Coatings Technol. 94–95 (1997) 21–26. doi:10.1016/S0257-8972(97)00470-2.

[2] L.C. Chen, C. Zhang, Z.G. Yang, Effect of pre-oxidation on the hot corrosion of CoNiCrAlYRe alloy, Corros. Sci. 53 (2011) 374–380. doi:10.1016/j.corsci.2010.09.045.

[3] J.G. Smeggil, Some comments on the role of yttrium in protective oxide scale adherence, Mater. Sci. Eng. 87 (1987) 261–265. doi:10.1016/0025-5416(87)90387-9.

[4] F.H. Stott, G.C. Wood, Growth and adhesion of oxide scales on Al2O3-forming alloys and coatings, Mater. Sci. Eng. 87 (1987) 267–274. doi:10.1016/0025-5416(87)90388-0.

[5] B.A. Pint, K.L. More, I.G. Wright, Effect of Quaternary Additions on the Oxidation Behavior of Hf-Doped NiAl, Oxid. Met. 59 (2003) 257–283.

doi:10.1023/A:1023087926788.

[6] H. Guo, Y. Cui, H. Peng, S. Gong, Improved cyclic oxidation resistance of electron beam physical vapor deposited nano-oxide dispersed β-NiAl coatings for Hf-containing superalloy, Corros. Sci. 52 (2010) 1440–1446. doi:10.1016/J.CORSCI.2010.01.009.

[7] T.A. Taylor, D.F. Bettridge, Development of alloyed and dispersion-strengthened MCrAlY coatings, Surf. Coatings Technol. 86–87 (1996) 9–14. doi:10.1016/S0257-8972(96)02961-1.

[8] N. Czech, F. Schmitz, W. Stamm, Improvement of MCrAlY coatings by addition of rhenium, Surf. Coatings Technol. 68–69 (1994) 17–21. doi:10.1016/0257-8972(94)90131-7.

[9] R. MEVREL, Cyclic oxidation of high-temperature alloys, Mater. Sci. Technol. 3 (n.d.) 531–535. http://cat.inist.fr/?aModele=afficheN&cpsidt=8330976 (accessed October 20, 2016).

[10] M. Tanno, K. Ogawa, T. Shoji, Effect of Cerium and Silicon Additions to MCrAlY on the High-Temperature Oxidation Behavior and Bond Strength of Thermal Barrier Coatings, Key Eng. Mater. 261–263 (2004) 1061–1066. doi:10.4028/www.scientific.net/KEM.261-263.1061.

[11] T. Amano, T. Taguchi, Spalling of the surface oxide formed on Ni-(20,40,60,80)Cr alloys with small additions of Ce and Si, J. Alloys Compd. 193 (1993) 20–22. doi:10.1016/0925-8388(93)90297-Z.

[12] Y. Itoh, M. Tamura, Reaction Diffusion Behaviors for Interface Between Ni-Based Super Alloys and Vacuum Plasma Sprayed MCrAlY Coatings, Trans. ASME. 121 (1999) 476–483. %5C%5CKwi-server%5Cliteratur%5Cedo%5Carticles%5CDR%5CDR_0094.pdf%5Cn%5C%5CKwi-server%5Cliteratur%5Cedo%5Carticles_ocrtxt%5CDR%5CDR_0094.txt.

[13] K. Yuan, R. Eriksson, R. Lin Peng, X.H. Li, S. Johansson, Y.D. Wang, MCrAlY coating design based on oxidation-diffusion modelling. Part I: Microstructural evolution, Surf. Coatings Technol. 254 (2014) 79–96. doi:10.1016/j.surfcoat.2014.05.067.

[14] S. Salam, P.Y. Hou, Y.D. Zhang, H.F. Wang, C. Zhang, Z.G. Yang, Compositional

effects on the high-temperature oxidation lifetime of MCrAlY type coating alloys, Corros. Sci. 95 (2015) 143–151. doi:10.1016/j.corsci.2015.03.011.

[15] Y. Wang, H.B. Guo, H. Peng, L.Q. Peng, S.K. Gong, Diffusion barrier behaviors of (Ru,Ni)Al/NiAl coatings on Ni-based superalloy substrate, Intermetallics. 19 (2011) 191–195. doi:10.1016/j.intermet.2010.08.016.

[16] A. Sato, H. Harada, T. Yokokawa, T. Murakumo, Y. Koizumi, T. Kobayashi, et al., The effects of ruthenium on the phase stability of fourth generation Ni-base single crystal superalloys, Scr. Mater. 54 (2006) 1679–1684. doi:10.1016/j.scriptamat.2006.01.003.

[17] T.J. Nijdam, W.G. Sloof, Effect of reactive element oxide inclusions on the growth kinetics of protective oxide scales, Acta Mater. 55 (2007) 5980–5987. doi:10.1016/j.actamat.2007.07.007.

[18] K.L. Luthra, C.L. Briant, Mechanism of adhesion of alumina on MCrAlY alloys, Oxid. Met. 26 (1986) 397–416. doi:10.1007/BF00659344.

[19] K. Yuan, R. Lin Peng, X.H. Li, S. Johansson, Y.D. Wang, Some aspects of elemental behaviour in HVOF MCrAlY coatings in high-temperature oxidation, Surf. Coatings Technol. 261 (2015) 86–101. doi:10.1016/j.surfcoat.2014.11.053.

[20] K. Yuan, R. Eriksson, R. Lin Peng, X.H. Li, S. Johansson, Y.D. Wang, Modeling of microstructural evolution and lifetime prediction of MCrAlY coatings on nickel based superalloys during high temperature oxidation, Surf. Coatings Technol. 232 (2013) 204–215. doi:10.1016/j.surfcoat.2013.05.008.

[21] R. Eriksson, K. Yuan, X.-H. Li, R. Lin Peng, MCrAlY coating design based on oxidation–diffusion modelling. Part II: Lifing aspects, Surf. Coatings Technol. 253 (2014) 27–37. doi:10.1016/j.surfcoat.2014.05.010.

[22] J. Yang, Q. Zheng, H. Zhang, X. Sun, H. Guan, Z. Hu, Effects of heat treatments on the microstructure of IN792 alloy, Mater. Sci. Eng. A. 527 (2010) 1016–1021. doi:10.1016/j.msea.2009.10.026.

[23] S. Saeidi, K.T. Voisey, D.G. McCartney, The effect of heat treatment on the oxidation behavior of HVOF and VPS CoNiCrAlY coatings, J. Therm. Spray Technol. 18 (2009) 209–216. doi:10.1007/s11666-009-9311-8.

[24] Thermo-Calc Software TCS Ni-based Superalloys Database version 8, (2015).

[25] Thermo-Calc Software TCS Ni- alloys Mobility Database version 4, (2015).

[26] J.O. Andersson, T. Helander, L. Hoglund, P. Shi, B. Sundman, THERMO-CALC & DICTRA, Computational Tools For Materials Science, Calphad. 26 (2002) 273–312. www.thermocalc.com.

[27] H. Larsson, R.C. Reed, On the numerical simulation of diffusion-controlled reactions under local equilibrium conditions, Acta Mater. 56 (2008) 3754–3760. doi:10.1016/j.actamat.2008.04.008.

[28] H. Larsson, A model for 1D multiphase moving phase boundary simulations under local equilibrium conditions, Calphad Comput. Coupling Phase Diagrams Thermochem. 47 (2014) 1–8. doi:10.1016/j.calphad.2014.06.001.

[29] J. Toscano, R. Va??en, A. Gil, M. Subanovic, D. Naumenko, L. Singheiser, et al., Parameters affecting TGO growth and adherence on MCrAlY-bond coats for TBC's, Surf. Coatings Technol. 201 (2006) 3906–3910. doi:10.1016/j.surfcoat.2006.07.247.

[30] X. Liu, L. Huang, Z.B. Bao, H. Wei, X.F. Sun, H.R. Guan, et al., Oxidation behavior of graded NiCrAlYRe coatings at 900, 1000 and 1100 °c, Oxid. Met. 71 (2009) 125–142. doi:10.1007/s11085-008-9131-0.

[31] M.W. Brumm, H.J. Grabke, The oxidation behaviour of NiAl-I. Phase transformations in the alumina scale during oxidation of NiAl and NiAl-Cr alloys, Corros. Sci. 33 (1992) 1677–1690. doi:10.1016/0010-938X(92)90002-K.

[32] G.C. Rybicki, J.L. Smialek, Effect of the theta-alpha-Al2O3 transformation on the oxidation behavior of beta-NiAl + Zr, Oxid. Met. 31 (1989) 275–304. doi:10.1007/BF00846690.

[33] J. Doychak, J.L. Smialek, C.A. Barrett, The oxidation of Ni-rich Ni-Al intermetallics, (1988). https://ntrs.nasa.gov/search.jsp?R=19890005862.

[34] B.A. Pint, On the Formation of Interfacial and Internal Voids in a-Al203 Scales, Oxid. Met. 48 (1997) 24–27. doi:10.1007/BF01670505.

[35] M.P. Brady, High-temperature oxidation and corrosion of metals, in: Mater. Sci. Technol., Wiley-VCH Verlag GmbH & Co. KGaA, 2008: pp. 229–325.

[36] D. Naumenko, B. Gleeson, E. Wessel, L. Singheiser, W.J. Quadakkers, Correlation between the microstructure, growth mechanism, and growth kinetics of alumina

scales on a FeCrAlY alloy, in: Metall. Mater. Trans. A Phys. Metall. Mater. Sci., 2007: pp. 2974–2983. doi:10.1007/s11661-007-9342-z.

[37] P. Burtin, J.P. Brunelle, M. Pijolat, M. Soustelle, Influence of surface area and additives on the thermal stability of transition alumina catalyst supports. I: Kinetic data, Appl. Catal. 34 (1987) 225–238. doi:10.1016/S0166-9834(00)82458-6.

[38] L. Lelait, S. Alpérine, R. Mévrel, Alumina scale growth at zirconia-MCrAlY interface: a microstructural study, J. Mater. Sci. 27 (1992) 5–12. doi:10.1007/BF02403637.

[39] M.H. Li, Z.Y. Zhang, X.F. Sun, J.G. Li, F.S. Yin, W.Y. Hu, et al., Oxidation behavior of sputter-deposited NiCrAlY coating, Surf. Coatings Technol. 165 (2003) 241–247. doi:10.1016/S0257-8972(02)00738-7.

[40] A.E. Paladino, W.D. Kingery, Aluminum Ion Diffusion in Aluminum Oxide, J. Chem. Phys. 37 (1962) 957. doi:10.1063/1.1733252.

[41] T.A. Ramanarayanan, M. Raghavan, R. Petkovic-Luton, Metallic yttrium additions to high temperature alloys: Influence on Al2O3 scale properties, Oxid. Met. 22 (1984) 83–100. doi:10.1007/BF00656898.

[42] K. Ogawa, K. Ito, T. Shoji, D.W. Seo, H. Tezuka, H. Kato, Effects of Ce and Si Additions to CoNiCrAlY Bond Coat Materials on Oxidation Behavior and Crack Propagation of Thermal Barrier Coatings, J. Therm. Spray Technol. 15 (2006) 640–651. doi:10.1361/105996306X147081.

Table 1 Chemical composition of heat-treated Ni27Co15Cr12.5AlX coatings [in wt. %].

MCrAlX with X=	Ru	Ce	Y	Others
C1	3.3	-	0.3	0.3Si, Mo,Ta<0.6
C2	-	0.2	-	

Table 2 Conditions of oxidation test (Iso-isothemal oxidation).

Condition	Time/Cycles
Iso-900 °C	500, 1500, 5000 h
Iso-1000 °C	500, 1500, 5000 h
Iso-1100 °C	50, 300, 500, 800 h
Cyclic oxidation	50, 300, 500, 800 cycles

Table 3 The composition (wt. %) of γ and β phase in S1 and S2 systems for short-range diffusion modelling.

	phase	Ni	Co	Cr	Al	Ru
S1	γ	36.3	33.3	24.7	3.8	1.9
	β	51.5	17.3	7.4	17.5	6.3
S2	γ	41.5	32.4	22	4.1	-
	β	56.8	18.6	6.8	17.8	-

Table 4 Al and Ru concentration (wt. %) in γ and β phase from EDS measurement. (Ratio = element concentration in phase/average value)

Element	Average content measured in the coatings	γ		β	
		wt.%	ratio	wt.%	ratio
Al (in C1)	11.5	3.8	0.33	17.5	1.52
Al (in C2)	12	4.1	0.34	17.8	1.48
Ru (in C1)	3.7	1.9	0.41	6.3	1.62

Preprints (www.preprints.org) | NOT PEER-REVIEWED | Posted: 14 March 2018 doi:10.20944/preprints201803.0105.v1

Peer-reviewed version available at *Coatings* **2018**, *8*, 129; doi:10.3390/coatings8040129

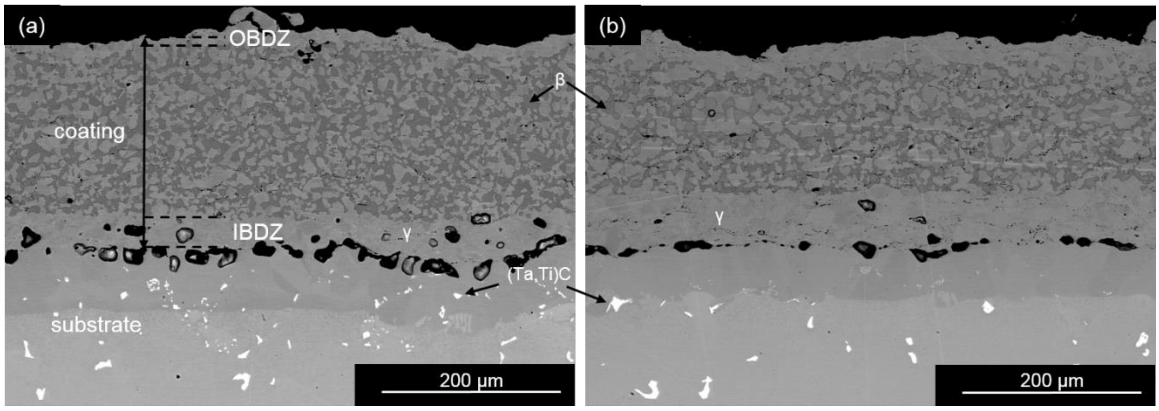

Fig. 1. BSE image showing microstructure of the C1 (a) and C2 (b) coating of isothermal 1100 °C specimen after 800 h oxidation..

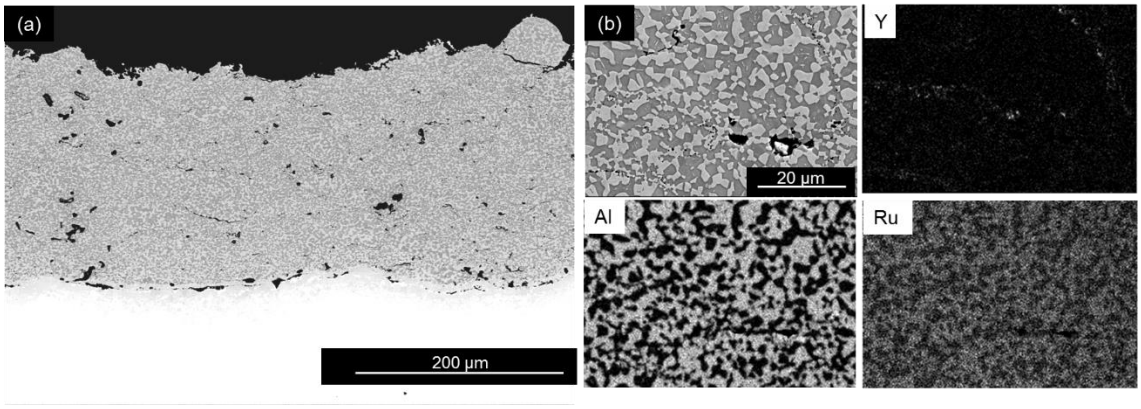

Fig. 2. BSE image showing the cross section of heat-treated coating of C1 (a) and EDS mapping of Y, Al and Ru in the as heat treated coating (b).

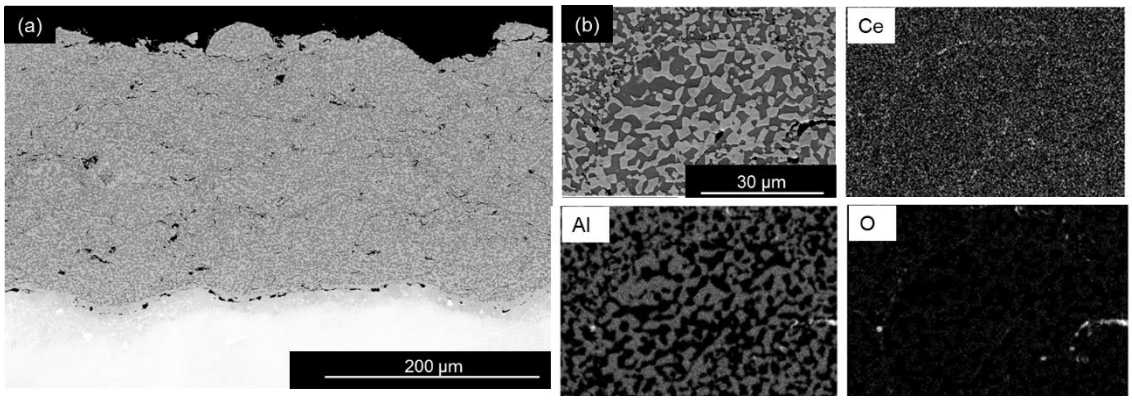

Fig. 3. BSE image showing the cross section of heat-treated coating of C2 (a) and EDS mapping of Ce, Al and O in the as heat treated coating (b).

Preprints (www.preprints.org) | NOT PEER-REVIEWED | Posted: 14 March 2018 doi:10.20944/preprints201803.0105.v1

Peer-reviewed version available at *Coatings* **2018**, *8*, 129; doi:10.3390/coatings8040129

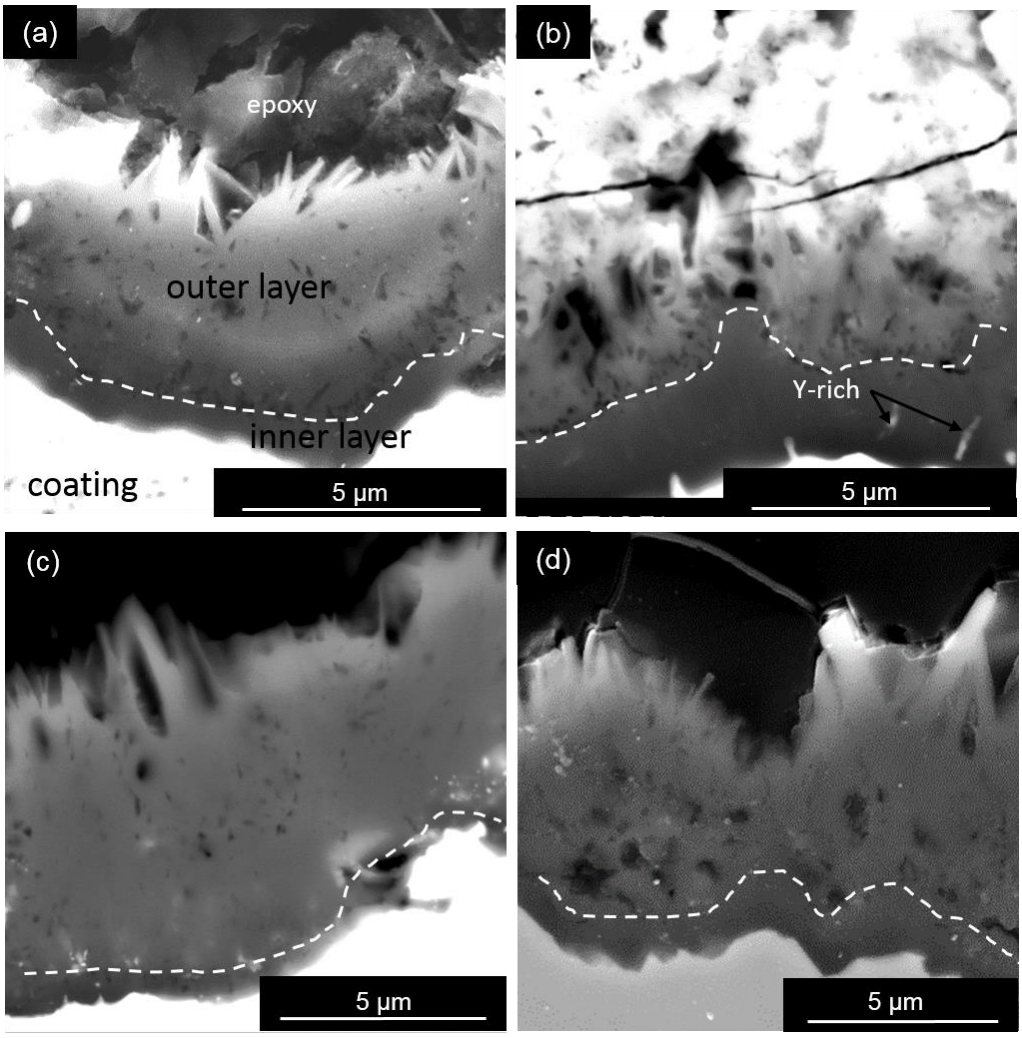

Fig. 4. Cross section of TGO after isothermal oxidation at 900 °C, Y+Ru doped C1 coating for 500 h (a) and 5000 h (b); Ce doped C2 coating for 500 h (c) and 5000 h (d). White dash lines marked the outer/inner Al_2O_3 layer boundary. (Note that the images are in different magnifications, white contrast in (b) is due to charging problem)

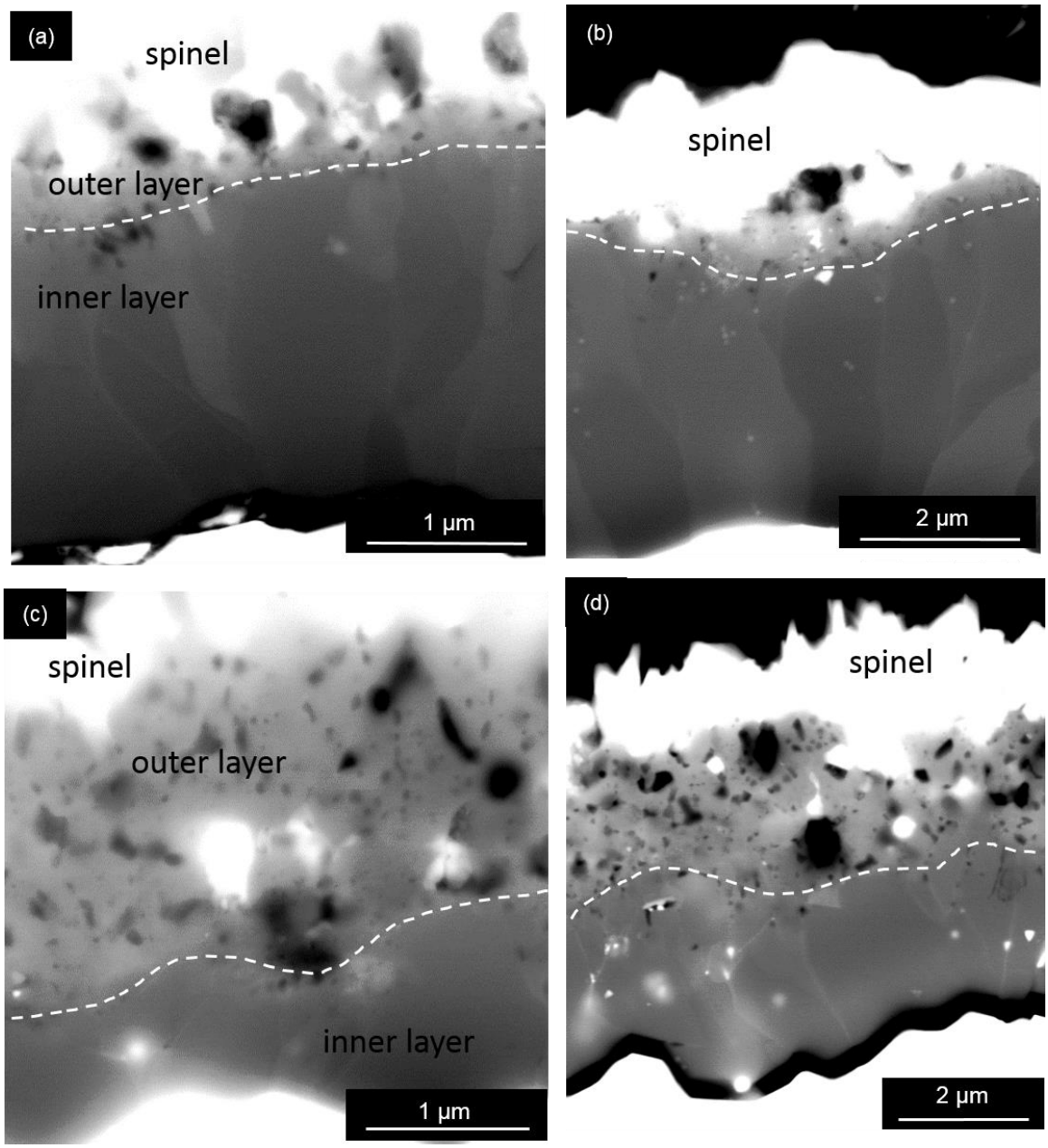

Fig. 5. Cross section of TGO after isothermal oxidation at 1000 °C, Y+Ru doped C1 coating for 500 h (a) and 5000 h (b); Ce doped C2 coating for 500 h (c) and 5000 h (d). White dash lines marked the outer/inner Al_2O_3 layer boundary. (Note that the images are in different magnifications.)

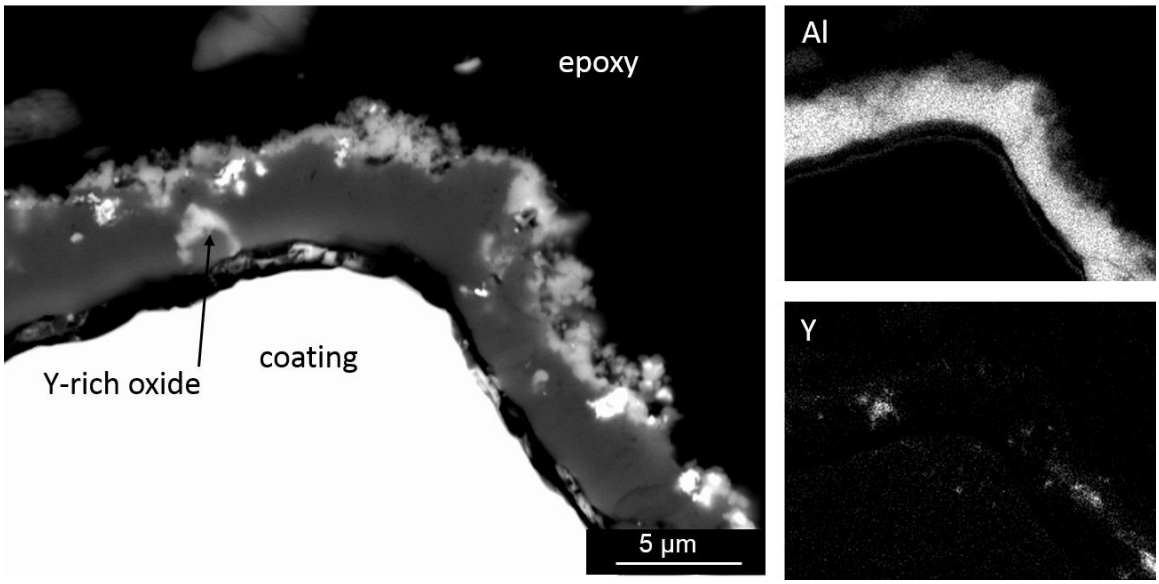

Fig. 6. EDS mapping on TGO of the C1 coating after isothermal oxidation at 1000 °C for 5000 h, showing Y rich particles.

Preprints (www.preprints.org) | NOT PEER-REVIEWED | Posted: 14 March 2018 doi:10.20944/preprints201803.0105.v1

Peer-reviewed version available at *Coatings* **2018**, *8*, 129; doi:10.3390/coatings8040129

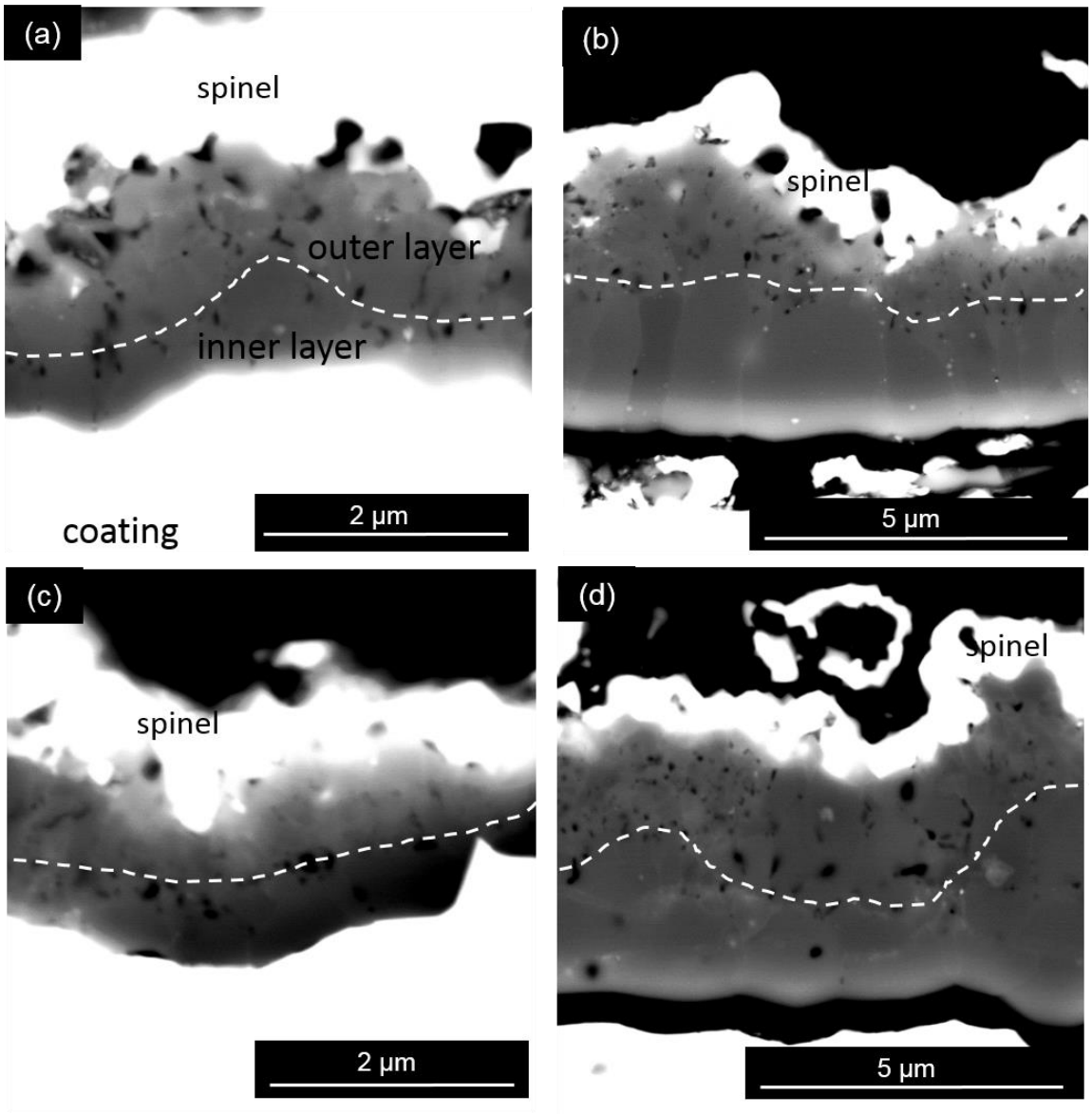

Fig. 7. Cross section of TGO after isothermal oxidation at 1100 ºC, Y+Ru doped C1 coating for 50 h (a) and 800 h (b); Ce doped C2 coating for 50 h (c) and 800 h (d). White dash lines marked the outer/inner Al_2O_3 layer boundary. (Note that the images are in different magnifications.)

Preprints (www.preprints.org) | NOT PEER-REVIEWED | Posted: 14 March 2018 doi:10.20944/preprints201803.0105.v1

Peer-reviewed version available at Coatings 2018, 8, 129; doi:10.3390/coatings8040129

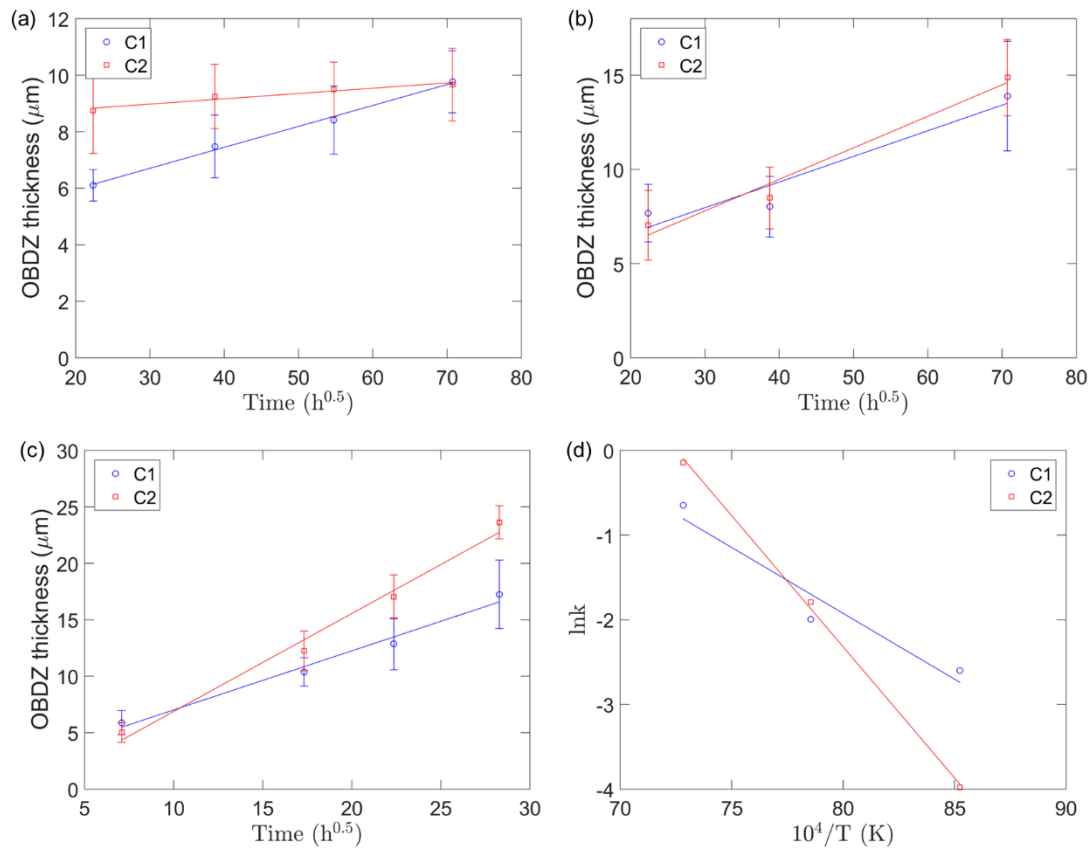

Fig. 8. The OBDZ thickness evolution of the C1 and C2 coatings after isothermal 900 °C (a), 1000 °C (b), 1100 °C (c) oxidation test and (d) Arrhenius relationship: ln(k) of C1 and C2 coatings for the isothermal oxidation at 900, 1000 and 1100 °C vs. $10^4/T$.

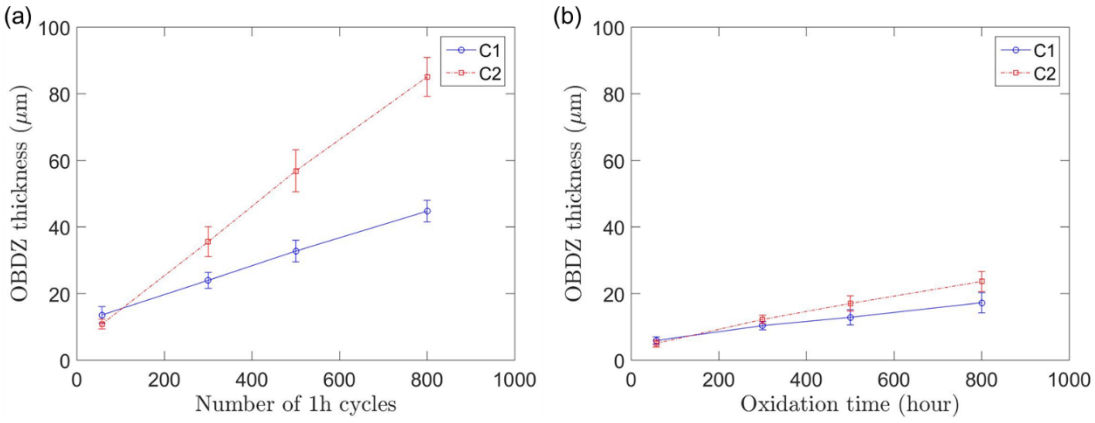

Fig. 9. The OBDZ thickness of the C1 and C2 coatings after cyclic oxidation testing at 1100 °C (a), and isothermal oxidation testing at 1100 °C (b).

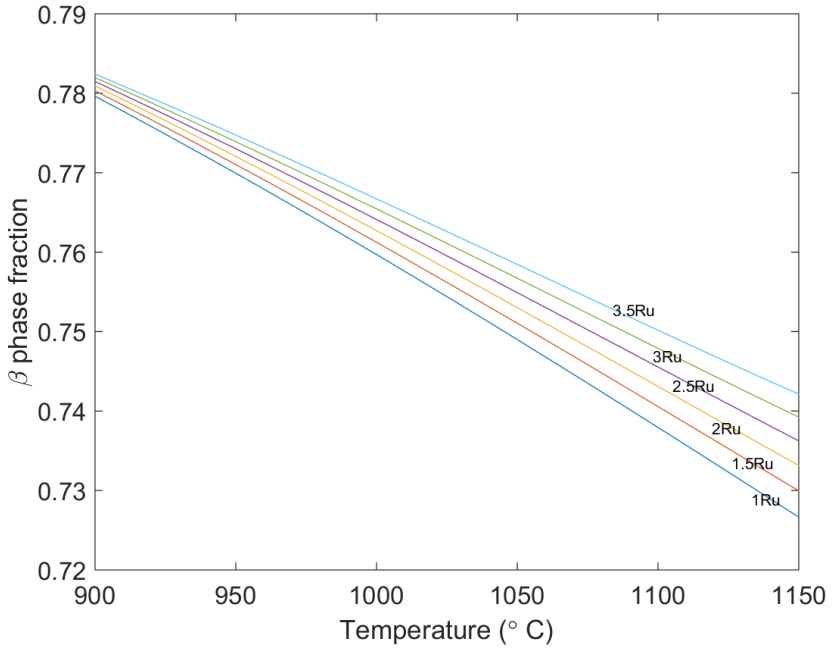

Fig. 10. β phase fraction for different alloy system from 900 to 1250 °C, derived from equilibrium calculation by Thermo-Calc. The composition of alloy systems are Ni27Co15Cr12.5Al+1Ru, 1.5Ru, 2Ru, 2.5Ru, 3Ru, 3.5Ru.

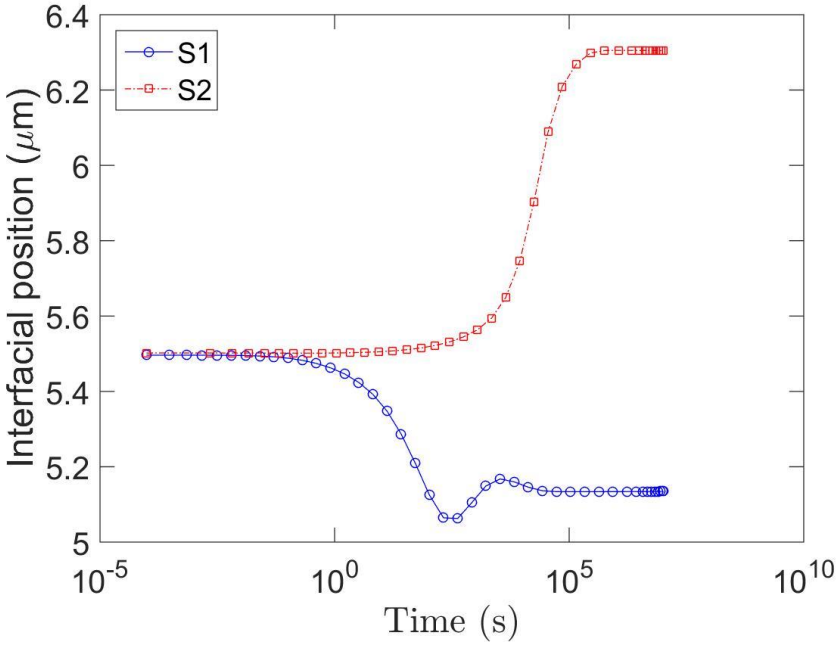

Fig. 11. The movement of γ/β phase region interfacial position from γ phase region (0-5.5 μm) into β phase region (5.5-10 μm) at 1100 ^{0}C, the original phase boundary was at 5.5 μm.

Preprints (www.preprints.org) | NOT PEER-REVIEWED | Posted: 14 March 2018 doi:10.20944/preprints201803.0105.v1

Peer-reviewed version available at Coatings 2018, 8, 129; doi:10.3390/coatings8040129

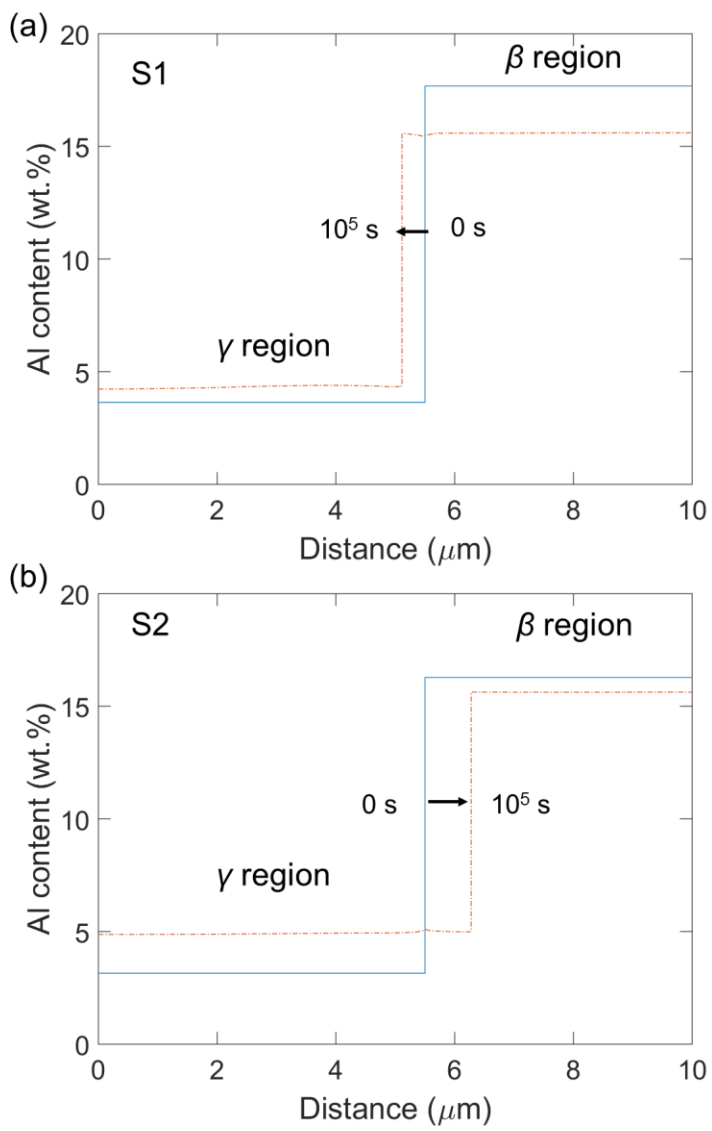

Fig. 12. Al concentration profile of S1 (a) and S2 (b) at 0 s and 10^5 s simulation time from moving phase boundary modelling. Al concentration profiles at other time were not included here for they were close to the data at 10^5 s. The γ phase region and β phase region were arranged from left to right with the interface at distance= 5.5 μm.

Preprints (www.preprints.org) | NOT PEER-REVIEWED | Posted: 14 March 2018 doi:10.20944/preprints201803.0105.v1

Peer-reviewed version available at Coatings 2018, 8, 129; doi:10.3390/coatings8040129

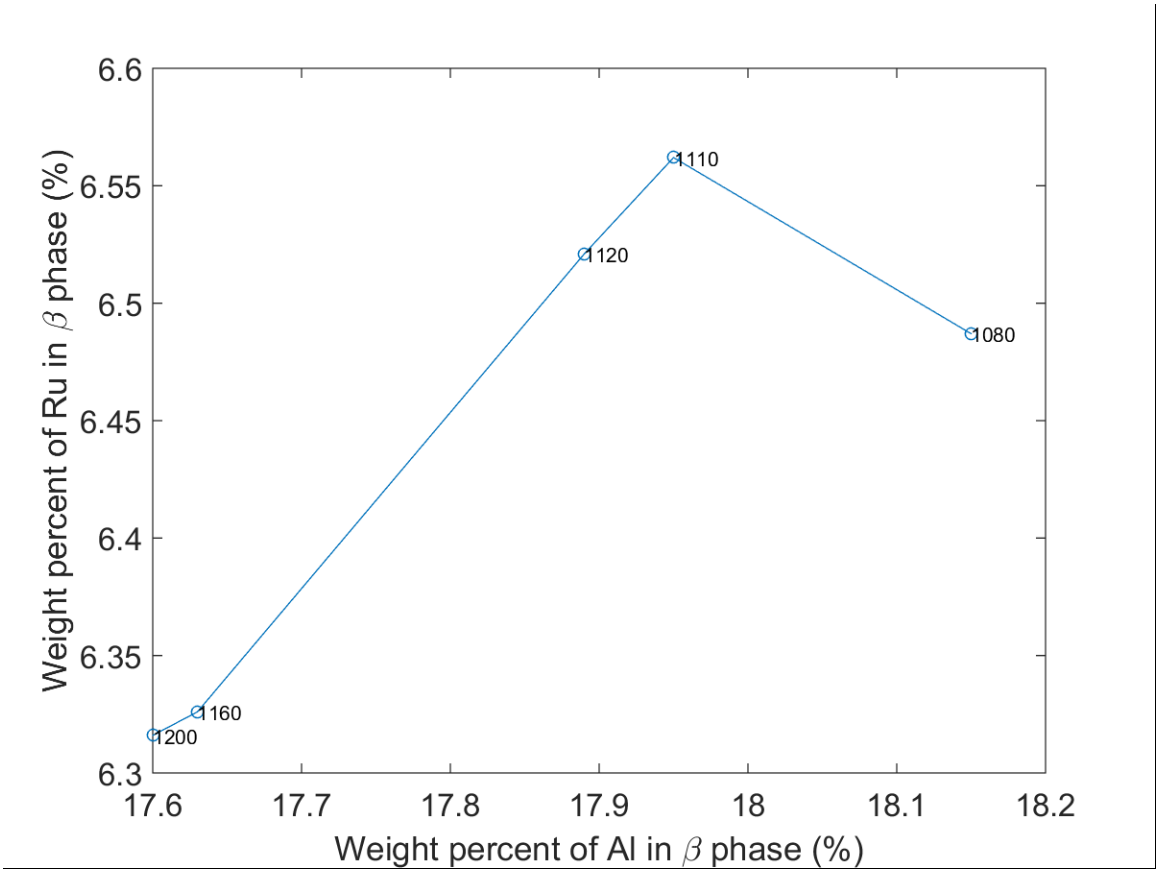

Fig. 13. Projection of three-dimensional diagram with weight percent of Al in β phase - x axis, Ru in β phase – y axis and temperature – z axis. The temperature corresponding to each point has been marked.

Preprints (www.preprints.org) | NOT PEER-REVIEWED | Posted: 14 March 2018 doi:10.20944/preprints201803.0105.v1

Peer-reviewed version available at Coatings 2018, 8, 129; doi:10.3390/coatings8040129

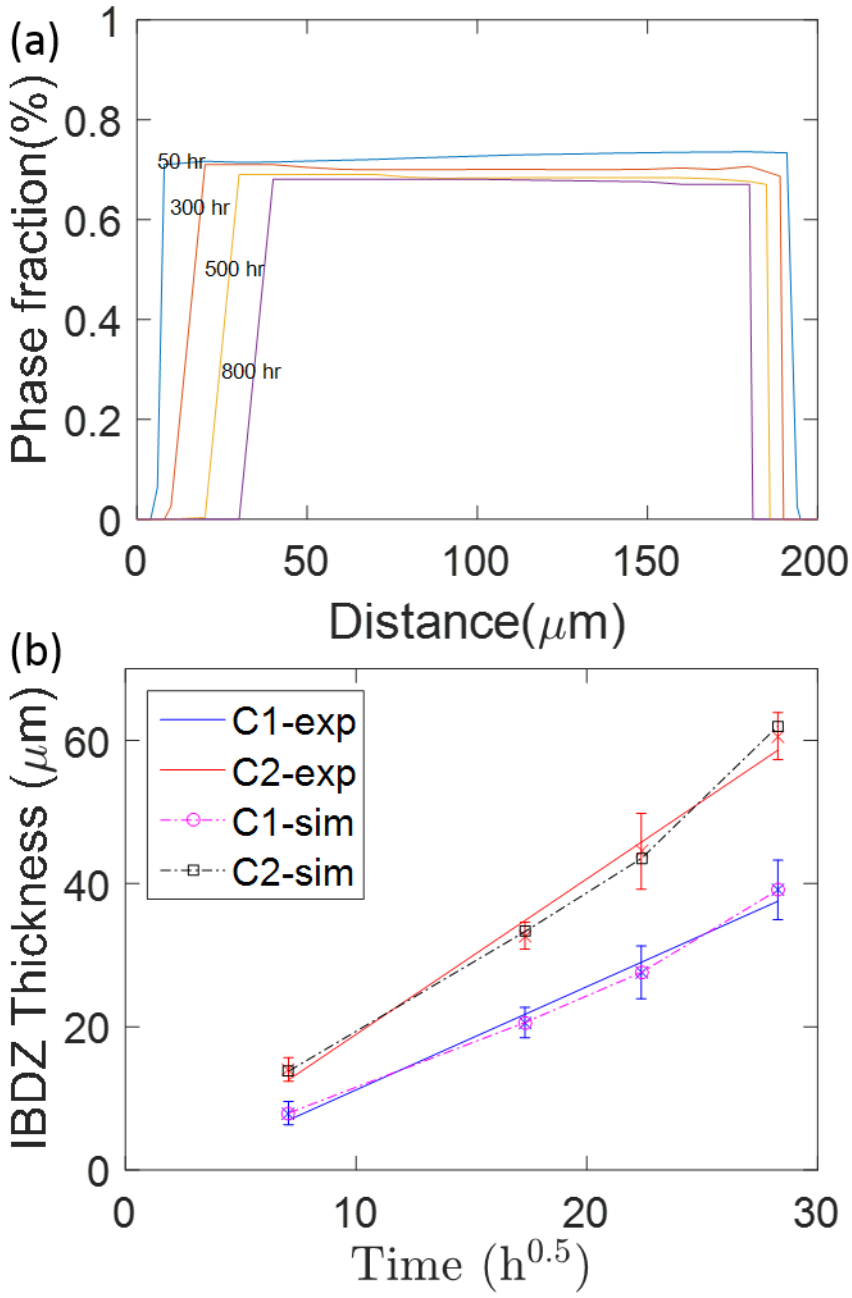

Fig. 14. Simulation results of inner-β phase depletion of Y+Ru-doped C1 coating at 1100 °C (a), IBDZ thickness data of C1 and C2 coating from isothermal oxidation test and simulation at 1100 °C plotted against square root of time (b), the dot line and solid line represented simulation results and isothermal oxidation test, respectively.